The Journal of Immunology

Ca2+ Release from the Endoplasmic Reticulum of NY-ESO-1 Specific T Cells Is Modulated by the Affinity of TCR and by the Use of the CD8 Coreceptor

Ji-Li Chen, Anthony J. Morgan, Guillaume Stewart-Jones, Dawn Shepherd, Giovanna Bossi, Linda Wooldridge, Sarah L. Hutchinson, Andrew K. Sewell, Gillian M. Griffiths, P. Anton van der Merwe, E. Yvonne Jones, Antony Galione and Vincenzo Cerundolo

J. Immunol. 2010;184;1829-1839; originally published online Jan 6, 2010;
doi:10.4049/jimmunol.0902103
http://www.jimmunol.org/cgi/content/full/184/4/1829

The Journal of Immunology is published twice each month by The American Association of Immunologists, Inc., 9650 Rockville Pike, Bethesda, MD 20814-3994.

Print ISSN: 0022-1767 Online ISSN: 1550-6606.

Ca^{2+} Release from the Endoplasmic Reticulum of NY-ESO-1–Specific T Cells Is Modulated by the Affinity of TCR and by the Use of the CD8 Coreceptor

Ji-Li Chen,*[,1] Anthony J. Morgan,[†,1] Guillaume Stewart-Jones,[‡] Dawn Shepherd,* Giovanna Bossi,[§] Linda Wooldridge,[¶] Sarah L. Hutchinson,* Andrew K. Sewell,[¶] Gillian M. Griffiths,[‖] P. Anton van der Merwe,[#] E. Yvonne Jones,[‡] Antony Galione,[†] and Vincenzo Cerundolo*

Although several cancer immunotherapy strategies are based on the use of analog peptides and on the modulation of the TCR affinity of adoptively transferred T cells, it remains unclear whether tumor-specific T cell activation by strong and weak TCR stimuli evoke different Ca^{2+} signatures from the Ca^{2+} intracellular stores and whether the amplitude of Ca^{2+} release from the endoplasmic reticulum (ER) can be further modulated by coreceptor binding to peptide/MHC. In this study, we combined functional, structural, and kinetic measurements to correlate the intensity of Ca^{2+} signals triggered by the stimulation of the 1G4 T cell clone specific to the tumor epitope NY-ESO-$1_{157–165}$. Two analogs of the NY-ESO-$1_{157–165}$ peptide, having similar affinity to HLA-A2 molecules, but a 6-fold difference in binding affinity for the 1G4 TCR, resulted in different Ca^{2+} signals and T cell activation. 1G4 stimulation by the stronger stimulus emptied the ER of stored Ca^{2+}, even in the absence of CD8 binding, resulting in sustained Ca^{2+} influx. In contrast, the weaker stimulus induced only partial emptying of stored Ca^{2+}, resulting in significantly diminished and oscillatory Ca^{2+} signals, which were enhanced by CD8 binding. Our data define the range of TCR/peptide MHC affinities required to induce depletion of Ca^{2+} from intracellular stores and provide insights into the ability of T cells to tailor the use of the CD8 coreceptor to enhance Ca^{2+} release from the ER. This, in turn, modulates Ca^{2+} influx from the extracellular environment, ultimately controlling T cell activation. ***The Journal of Immunology*****, 2010, 184: 1829–1839.**

An important question for the optimization of vaccination strategies concerns the nature of the developmental programs, and consequent functional profiles, invoked by TCR triggering by agonists, superagonists, and weak peptide agonists. Because natural tumor Ags elicit relatively weak T cell responses, two approaches currently being investigated are the optimization of the MHC class I anchor residues in tumor epitopes, to enhance binding of the peptide to the MHC class I molecule (1–3), and site-directed mutagenesis of TCRs to enhance T cell effector function of adoptively transferred T cells (4). Although in vitro and in vivo data with peptide analogs and mutagenized TCR showed larger Ag-specific CTL expansions than T cell proliferation obtained with wild-type peptides (5, 6) or wild-type TCRs (7), the use of peptide agonists and mutated TCRs in clinical applications needs to be carefully monitored, because such strategies may result in the loss of Ag specificity due to the enhanced T cell reactivity, as reviewed by Iero et al. (8). Recent results have extended this notion by demonstrating Ag cross-reactivity when $CD8^+$ T cells were transfected with a higher-affinity variant of the NY-$ESO_{157–165}$ A2-restricted 1G4 TCR (7), whereas the same soluble higher-affinity 1G4 TCR was capable of specifically recognizing NY-$ESO_{157–165}$-pulsed target cells (9).

The manner in which the intensity of TCR triggering is translated functionally is an active area of T cell research. In the last few years, it has become known that elevation of intracellular calcium (Ca^{2+}), a crucial early step in T cell activation, occurs within milliseconds of TCR engagement by peptide-MHC (pMHC) (10, 11). Binding of the TCR to the pMHC results in egress of Ca^{2+} from the endoplasmic reticulum (ER) into the cytosol (12), which, in turn, initiates Ca^{2+} influx into the cytosol from the extracellular environment, via the opening of calcium release-activated calcium/Orai1 channels located at the cell surface (13, 14). The amplitude and duration of the increase in Ca^{2+} influx modulates the strength and fitness of the T cell response and must be sustained for a prolonged period before gene expression and lymphokine production begin (15). It is known that the predominant route of Ca^{2+} influx into T cells is the store-operated Ca^{2+} entry (SOCE) pathway, which is regulated by the filling state of the ER (16). The use of altered peptide ligands showed that agonistic

*Weatherall Institute of Molecular Medicine, [†]Department of Pharmacology, [‡]Division of Structural Biology, Wellcome Trust Centre for Human Genetics, and [#]Sir William Dunn School of Pathology, University of Oxford, Oxford; [§]Immunocore, Abingdon, Oxon; [¶]Department of Infection, Immunity, and Biochemistry, Cardiff University School of Medicine, Cardiff; and [‖]Cambridge Institute for Medical Research, Addenbrooke's Hospital, Cambridge, United Kingdom

[1]J.-L.C. and A.J.M. contributed equally to this work.

Received for publication July 1, 2009. Accepted for publication December 5, 2009.

This work was supported by Cancer Research UK (C399/A2291), European Grant FP6 Cancer Immunotherapy, Oxford Biomedical Research Centre and Experimental Cancer Medical Centre, and the U.K. Medical Research Council. E.Y.J. is a Cancer Research UK Principal Research Fellow. A.J.M. and A.G. are funded by the Wellcome Trust.

Coordinates for the ESO-9L A2 crystal structure have been deposited in the Research Collaboratory for Structural Bioinformatics Protein Data Bank under accession number 3KLA.

Address correspondence and reprint requests to Prof. Vincenzo Cerundolo, Tumour Immunology Group, Nuffield Department of Medicine, Weatherall Institute of Molecular Medicine, OX3 9DS Oxford, U.K. E-mail address: vincenzo.cerundolo@imm.ox.ac.uk

The online version of this article contains supplemental material.

Abbreviations used in this paper: CPA, cyclopiazonic acid; ER, endoplasmic reticulum; IP_3, inositol 1,4,5-trisphosphate; MER, mean elevated ratio; NAADP, nicotinic acid adenine dinucleotide phosphate; PDB, Brookhaven Protein Data Bank; pMHC, peptide-MHC; SOCE, store-operated Ca^{2+} entry; SPR, surface plasmon resonance; STIM1, stromal interaction molecule 1.

peptides stimulate a cytosolic Ca^{2+} response composed of an initial small sinusoidal peak followed by a high response, whereas the signal evoked by weaker agonist peptides leads to an oscillatory response (17, 18). The strength of the TCR-pMHC also affects the speed of the Ca^{2+} responses, contributing to the extent of subsequent T cell proliferation (19). Although the SOCE model predicts that the greater the store release (and hence, emptying), the greater the Ca^{2+} influx, the relationship between the amount of Ca^{2+} influx and the release of Ca^{2+} from intracellular stores has not been addressed with Ag-specific T cell clones activated by peptide ligands with different TCR affinities.

In addition to the affinity of the TCR–pMHC interaction, binding of the CD4 and CD8 coreceptors to MHC class II or I molecules, respectively (20–22), can influence the overall avidity of the TCR–pMHC association (11, 22–25). Moreover, the CD4 and CD8 coreceptors are important for signal initiation because they associate to the tyrosine kinase Lck (26), which is required for critical early events in TCR signaling (27). It was shown that accumulation of the tyrosine kinase Lck at the immunological synapse is modulated by the strength of TCR binding to pMHC (28). Lck phosphorylates ITAMs, linking the Ag receptor to the downstream signaling machinery of the TCR CD3 molecules (29) and the tyrosine residues on the Syk family kinase ZAP70 (30, 31), thereby increasing the enzymatic activity of ZAP70 (32). Thus the coreceptor plays an important role in coupling ligand binding with the initiation of signal transduction.

Despite the large body of knowledge on Ca^{2+} influx in T cells, it remains unknown whether the release of Ca^{2+} from the intracellular stores, which are localized mainly in the ER (16), is modulated by the avidity of the TCR–pMHC interaction. To address this issue, we compared the release of Ca^{2+} from the ER and the subsequent influx of Ca^{2+} into the cytosol from the extracellular milieu after stimulation of a defined Ag-specific T cell clone (1G4 CTL) (33) by two HLA-A2 (A2)-bound peptide analogs, derived from the tumor Ag NY-ESO-$1_{157–165}$ peptide (SLLMWITQC) (2). Our data indicate that the strength of TCR binding to pMHC results in different degrees of Ca^{2+} release from the intracellular stores, which, in turn, drives a proportional Ca^{2+} influx. This effect is modulated by the binding of the CD8 coreceptor to MHC class I molecules, which can significantly enhance the amount of Ca^{2+} release from the intracellular stores triggered by both peptides and, in particular, by the weaker NY-ESO-$1_{157–165}$ peptide agonist.

Materials and Methods

Synthetic peptides

Peptides were synthesized by standard solid-phase chemistry on a multiple-peptide synthesizer (Sigma-Genosys, The Woodlands, TX) by using F-moc for transient N-terminal protection. All peptides were 99% pure as determined by analytical HPLC and mass spectrometry. Lyophilized NY-ESO-$1_{157–165}$ wild-type peptide (SLLMWITQC) and analog peptides containing a substitution of cysteine at position 165 of the NY-ESO-$1_{157–165}$ to valine (ESO 9V) or leucine (ESO 9L) were diluted in DMSO and stored at −20°C.

Immunoprecipitation

Aliquots of 14×10^7 T2 cells were labeled with 74 MBq [^{35}S] methionine for 23 min, washed twice with cold PBS, and resuspended in lysis buffer containing protease inhibitors (150 mM NaCl, 50 mM TrisHCl, pH 7.5, 5 mM EDTA, 1% Nonidet P-40, 2 mM PMSF, 5 mM iodoacetamide). After a 30-min peptide pulse at 4°C, the nuclei were removed, and the supernatant was precleared overnight at 4°C with 100 μl washed 10% (w/v) *Staphylococcus* A. BB7.2 Ab (15 μg/tube) was added for 90 min on ice, followed by 150 μl 5% (w/v) protein A-Sepharose (Sigma-Aldrich, Poole, U.K.). The tubes were rotated for 45 min and then the beads were washed four times with lysis buffer. The samples were eluted and analyzed on 12% polyacrylamide gels.

Flow cytometry

T2 cells (3×10^4) were pulsed with different concentrations of peptides for 2 h at 37°C. Cells were incubated with 40 μg/ml biotinylated F(ab′)$_2$ Abs for 30 min at 4°C and visualized by streptavidin-conjugated R-PE (Sigma-Aldrich) for 20 min at room temperature.

pMHC production

Residues 1–278 of the A2 H chain with the C terminus BirA tag were expressed in *Escherichia coli* as inclusion bodies, refolded, and purified with the NY-ESO-1 peptides SLLMWITQV or SLLMWITQL and β_2M as described previously (33).

Expression and purification of the 1G4 NY-ESO-1 TCR

The 1G4 TCR was refolded and purified from *E. coli*-derived inclusion bodies as described previously (33).

Surface plasmon resonance

Surface plasmon resonance (SPR) experiments were performed using a Biacore3000 (Biacore, Amersham, U.K.). Biotinylated soluble HLA (ligand) was immobilized on Streptavidin-coated CM5 chip (Biacore) at the level of 1,000 RU per flow cell. Equilibrium binding was measured at the flow rate of 5 μl/min, starting with the lowest analyte concentration. Binding responses were determined by subtracting responses obtained in reference flow cells with irrelevant pMHC immobilized. K_D values were calculated by fitting the 1:1 Langmuir binding isotherm to the data using Origin. Kinetics of TCR–pMHC interactions were measured at 30 μl/min, and the curves were fitted by global fitting of the standard 1:1 Langmuir binding model to the data (BIAevaluation software; Biacore).

Crystallization and x-ray diffraction data collection

All crystallizations were performed by the sitting drop vapor diffusion technique. Crystals of A2-ESO 9L complexes were grown to dimensions of $130 \times 80 \times 70$ μm at room temperature (21°C) from 2 μl protein (at 10 mg/ml) + 2 μl mother liquor (14% polyethylene glycol 8000, 50 mM MES, pH 6.5) drops. Crystals were cryoprotected by sequential transfer into reservoir solutions containing 10% and 20% glycerol and were flash-cooled and maintained at 100 K, using a cryostream (Oxford Cryosystems, Oxford, U.K.). High-resolution data for the A2-ESO 9L complex were collected at station ID14 EH2 of the European Synchrotron Radiation Facility (Grenoble, France) with a Quantum 4 CCD detector (Area Detector Systems Corporation, Porway, CA). Datasets were auto-indexed and integrated with the program DENZO (www.hkl-xray.com; HKL Research, Charlottesville, VA) (34), followed by scaling with the program SCALEPACK (HKL Research) (34); the results are summarized in Supplemental Table I.

Crystal structure determination, refinement, and analysis

The HLA-A*0201-SLLMWITQL crystal structure (consisting of two A2-ESO 9L complexes per crystallographic asymmetric unit) was determined by molecular replacement using the CCP4 program Phaser (www.ccp4.ac.uk; University of Cambridge, Cambridge, U.K.) with a search model comprising a representative HLA-A*0201 complex crystal structure (Brookhaven Protein Data Bank [PDB] accession code 2V2X). Using the refinement algorithms in REFMAC5 [www.ccp4.ac.uk, (35)], the two A2-ESO 9L complexes were subjected to several rounds of rigid body refinement of individual domains. Then using the restrained translation/libration/screw vibrational motion refinement algorithms in REFMAC5, crystallographic conjugate gradient minimization refinement was performed, and manual refitting of the models was carried out using the Crystallographic Object-Oriented Toolkit [www.ccp4.ac.uk; York Structural Biology Laboratory, University of York, U.K., (36)]. Water picking was carried out with ARPw/ARP (European Bioinformatics Institute, Cambridge, U.K.) in the final stages of refinement (37). All regions of the A2-ESO 9L complex were visible as clear electron density and were included in the final models.

1G4:target cell conjugate measurements

T2 target cells were pulsed with 1 μM or 100, 10, or 5 nM ESO 9V or ESO 9L peptide for 1 h at 37°C and washed twice in PBS. 1G4 CTL and T2 cells were washed in PBS, and each cell pellet was resuspended to a final concentration of 5×10^5 cells/ml in RPMI 1640. 1G4 CTLs and target were mixed 1:1, left for 5 min in suspension, and then plated on glass multiwell slides and incubated for 30 min at 37°C. Cells were fixed in 100% methanol, precooled to −20°C, washed in PBS, and blocked in PBS, 2% BSA. The slides were mounted in PBS containing 90% glycerol and 2.5% 1,4-diazabicyclo[2.2.2]octane. Samples were examined using

a Bio-Rad Radiance 2000 MP laser-scanning microscope, and the conjugation rate and granule polarization were quantified using an Axioplan 2 epifluorescent microscope (Zeiss, Welwyn Garden City, U.K.).

Live cell video microscopy

1G4 CTLs (2×10^4) were incubated with 60 nM lysotracker green DND-26 (Invitrogen, Paisley, U.K.) for 1 h at 37°C in RPMI 1640 without phenol red, 5% human serum, 1mM HEPES. T2 target cells were pulsed with 1 μM ESO 9V peptide or ESO 9L peptide for 1 h at 37°C and washed twice in PBS. Target cells (2×10^4) were allowed to adhere on a glass coverslip mounted in a temperature-controlled chamber for 10 min at 37°C in RPMI 1640 without serum, without phenol red plus HEPES. Lysotracker green DND-26–labeled 1G4 NY-ESO-$1_{157–165}$ CTLs were added to the T2 cells in the chamber. Sequential confocal images were acquired every 20 s. A Nikon (Kingston on Thames, U.K.) TE300 microscope attached to a Radiance2000 MP laser-scanning microscope (Bio Rad, Hemel Hempstead, U.K.) was used, with a 488-nm and a 543-nm laser for epifluorescence and Nomarski differential interference contrast for the transmitted light. The images were processed using MetaMorph (Sunnyvale, CA) version 4.5 software.

ELISA assays

1G4 CTLs and peptide-pulsed target cells (A2 C1R or A2 227/8KA C1R) were incubated at 37°C for 4 h at an E:T ratio of 1:1, and the supernatant was harvested and assayed for MIP-1β and IFN-γ by ELISA (R&D Systems, Minneapolis, MN). Data shown are SD from the mean of two duplicate assays. For the detection of folded HLA-A2 tetramers (Supplemental Fig. 4), HLA-A2 tetramers were immobilized by binding to streptavidin-coated plates (Sigma M5432): 100 μl of serial 3-fold dilutions of pMHC (concentration 100 μg/ml to 500 pg/ml in blocking buffer; 10% FCS in PBS) were added/well, and plates were incubated for 1.5 h at 4°C. Plates were washed four times with PBS/0.5% Tween, incubated for 4 h at 37°C, and washed four times with wash buffer. Ab BB7.2 (4°C/well, concentration 10 μg/ml in blocking buffer) was added, and the plates were incubated overnight at 4°C. Following four washes in cold wash buffer, 100 μl a 1:1000 dilution (in blocking buffer) of goat anti-mouse IgG (DakoCytomation, Glostrup, Denmark) was added. Plates were incubated for 1 h at 4°C, washed six times, and 100 μl tetramethylbenzidine was added per well. The reaction was stopped with 50 μl 0.5 M H_2SO_4, and signals were quantitated using an ELISA plate reader.

^{51}Cr release assay

ESO peptide recognition was assessed using target cells (A2 C1R or A2 227/8KA C1R) labeled with ^{51}Cr for 90 min at 37°C and washed three times. Labeled target cells (5000 cells/100 μl) were added to U-bottom microwells in the presence or absence of peptides at different concentrations. ^{51}Cr release was measured after incubation for 4 h at 37°C. The percentage of specific lysis was calculated as: $100 \times$ [(experimental − spontaneous release)/(total − spontaneous release)].

Stimulation of 1G4 CTLs for subsequent immunoblotting

1G4 CTLs were washed twice in RPMI 1640 and incubated overnight in RPMI 1640 containing 10% FCS. FCS was washed off by two changes of RPMI 1640, and 1×10^6 1G4 CTLs were resuspended in 10 μl RPMI 1640. After 10 min at 37°C and 5% CO_2, 1G4 CTLs were stimulated by incubation with 1 μg/ml HLA-A2 tetramer loaded with ESO 9V, ESO 9C, or ESO 9L peptides for 3 min. The reaction was stopped by washing once with 0.5 ml ice-cold PBS and resuspending the pellet in cold lysis buffer (140 mm NaCl, 20 mm Tris, pH 8, 10 mM sodium fluoride, 2 mM EDTA, 20% glycerol, 1% IGEPAL, 1 mM Na_3VO_4, 10 μg/ml aprotinin, 10 μg/ml leupeptin) at 5×10^7 cells/ml.

Antiphosphotyrosine immunoblotting

1G4 CTLs were lysed on ice for 30 min, and the nuclear fraction was pelleted by centrifugation at $16{,}000 \times g$ for 15 min. The remaining lysate was aspirated and added to an equal volume of SDS loading buffer (350 mm Tris, pH 6.8, 350 mm SDS, 30% glycerol, 600 mm DTT, 175 μm bromophenol blue). After boiling for 6 min with agitation, the sample was separated by electrophoresis (100 V for 16 h) on a 12% SDS-PAGE gel. Proteins were transferred from the gel by electrophoresis at 25 V for 50 min. After transfer, protein bands on the nitrocellulose membrane were visualized by staining [0.1% (w/v) Ponceau S (Sigma-Aldrich) in 5% (v/v) glacial acetic acid (Sigma-Aldrich)] for 60 s with agitation, incubated with double-distilled water for 60 s with agitation, and drained. The membrane was incubated with sheep anti-mouse peroxidase-linked secondary Ab (Amersham Biosciences, Little Chalfont, U.K.; 1:2000 in wash buffer, 2.5% milk powder) for 1.5 h. After three additional washes, the blot was developed using chemiluminescent substrate Supersignal Pico (Perbio, Cramlington, U.K.). All washes and incubations with Abs were performed at 4°C.

Intracellular Ca^{2+} concentration measurements in 1G4 CTL clone

[Ca^{2+}] was monitored in the 1G4 CTL clone by fluorescence microscopy. 1G4 cells adhering to poly-lysine–coated glass coverslips were loaded with Ca^{2+}-sensitive fluorescent dye by incubating cells with RPMI 1640 containing 5 μM fluo-3/AM plus 0.03% (w/v) Pluronic F127 for 30 min at room temperature and mounted on the stage of a Zeiss LSM510 Meta confocal laser-scanning microscope (excitation 488 nm, emission > 505 nm) equipped with a ×63 objective. Target cells (wild-type C1R-A2 or mutant C1R-A2 227/8KA) were pulsed with 5 or 100 nM peptide (ESO 9V or ESO 9L) for 90 min at 37°C, washed twice with FCS-free RPMI 1640 medium (Sigma-Aldrich), and then added to the cell chamber. Experiments were conducted at room temperature with an image collected every 5 s.

Further validation of our [Ca^{2+}] recordings was obtained by repeating several experiments at 37°C and with the ratiometric dye fura 2. 1G4 CTLs were loaded with 5 μM fura 2-AM (plus 0.03% Pluronic F127) at room temperature for 30 min. Loaded 1G4 cells were then washed with RPMI 1640 prewarmed to 37°C and mounted on the heated stage of an Olympus IX71 microscope equipped with a ×40 UApo/340 objective (1.35 NA) and a 12-bit Photometrics Coolsnap HQ2 CCD camera. Cells were excited alternately by 340- and 380-nm light using a Cairn monochromator; emission data were collected at 480–540 nm using a bandpass filter. Data are expressed as the 340/380 ratio, which is proportional to the intracellular [Ca^{2+}]. By analogy with the analysis of the fluo-3 traces, the maximum amplitude and mean elevated ratio (340/380) were calculated on a single-cell basis.

Results

Kinetic analyses of the ESO 9V and ESO 9L binding to A2 molecules and the 1G4 TCR

The binding affinity of the ESO 9V and ESO 9L peptides, containing a substitution of cysteine at position 165 of the NY-ESO-$1_{157–165}$ to valine (ESO 9V) or leucine (ESO 9L), to A2 molecules was initially assessed by measuring peptide binding to metabolically labeled A2 molecules in T2 cells. OD measurements of metabolically labeled A2 eluted from SDS-containing polyacrylamide gels showed that ESO 9V and ESO 9L peptides stabilized A2 molecules with a comparable efficiency (Fig. 1*A*). To further validate these results, experiments were performed using the 3M4E5 F(ab′)$_2$ Ab specific to NY-ESO-$1_{157–165}$–A2 complexes (33). Initial Biacore measurements showed that the 3M4E5 F(ab′)$_2$ Ab recognized A2 molecules loaded with ESO 9V or ESO 9L peptide with a similar affinity (K_D) ~60 nM (data not shown). FACS staining of T2 cells pulsed with different concentrations of the ESO 9V and ESO 9L peptides with the 3M4E5 Ab confirmed that the ESO 9V and ESO 9L peptides bind to A2 molecules equally well (Fig. 1*B*).

In contrast, binding of the 1G4 TCR to A2 molecules loaded with the ESO 9V or the ESO 9L peptide demonstrated that the binding affinity of the 1G4 TCR for the A2-ESO 9V complex was six times higher than that for the A2-ESO 9L complex (Fig. 2). The equilibrium binding constants at 25°C for the soluble 1G4 TCR binding to A2 loaded with the ESO 9V or ESO 9L peptide were 5.5 and 31.1 μM, respectively (Fig. 2*C*, 2*D*). Kinetic measurements demonstrated that the 1G4 TCR-A2-ESO 9V complex has slower ligand dissociation ($t_{1/2}$ = 8.77 s^{-1}) than the 1G4 TCR-A2-ESO 9L complex ($t_{1/2}$ = 1.69 s^{-1}) (Fig. 2*A*, 2*B*). Analysis of the binding curves of conformation-specific anti–A2-peptide and anti-β_2M Abs confirmed that equivalent amounts of correctly refolded A2-peptide complexes were immobilized to the Biacore chips (Supplemental Fig. 1).

Crystal structure of A2-ESO 9L and A2-ESO 9V indicates alterations in the surface presented for TCR recognition

To explore the molecular basis for the similar affinity of ESO 9L and ESO 9V to A2 molecules and to gain insights into the mechanisms controlling the different affinity of binding to the 1G4

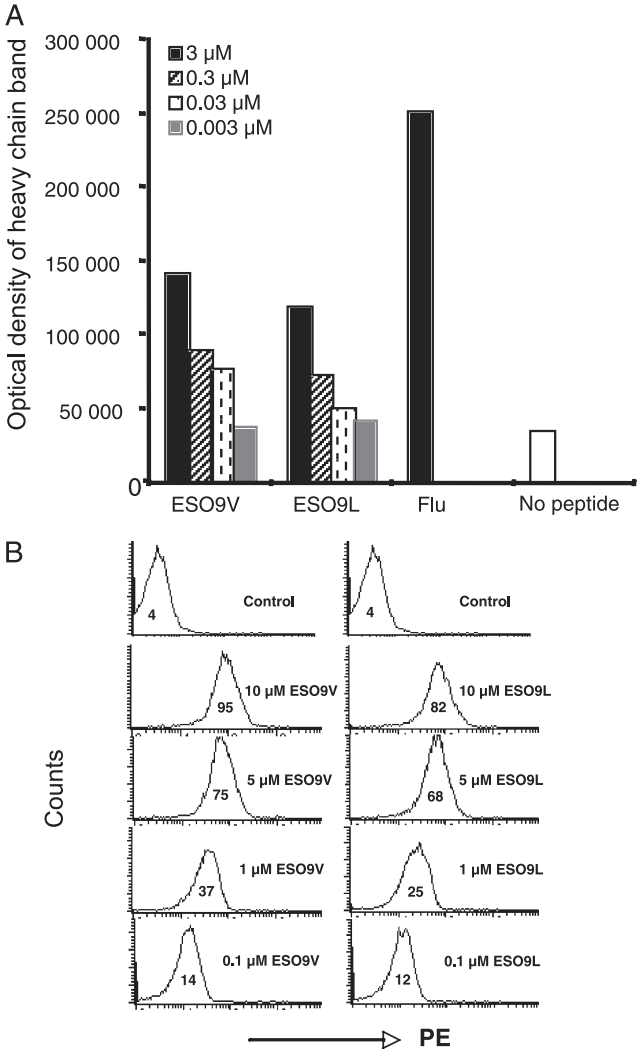

FIGURE 1. Binding measurements of peptide to A2 molecules. *A*, T2 cells were pulsed with ESO 9V or ESO 9L peptide at the concentrations indicated, and the HLA-A2-peptide complexes were precipitated. HLA-A2 molecules from T2 cells pulsed with 3 μM influenza virus matrix 58–66 peptide or in the absence of peptide were used as positive and negative controls, respectively. *B*, T2 cells were stained with the A2-ESO 9C-specific $F(ab')_2$ Ab 3M4E5. T2 cells were pulsed with ESO 9V (*left panels*) or ESO 9L (*right panels*) peptide at the concentrations indicated and then stained with the A2-ESO 9C-specific $F(ab')_2$. Negative control cells were pulsed with the influenza virus matrix peptide. Data are mean channel fluorescence.

TCR, we determined the crystal structure of the A2-ESO 9L complex at 1.7 Å resolution. Comparison of this high-resolution structure with those previously reported for A2-ESO 9C (38) and the 1G4 TCR-A2-ESO 9V complex (33) revealed changes in the surface presented for TCR recognition that were the indirect result of the substitution of the P9 anchor side chain. These changes are triggered by the larger size of the leucine side chain compared with those of cysteine and valine. The F pocket in A2 can accommodate valine or leucine; however, in previously reported structures, the latter choice of anchor residue triggers a local rearrangement of the binding groove residues, expanding the volume of the F pocket to match the longer side chain (Fig. 3). This rearrangement requires a concerted switch in side chain conformation by A2 binding groove residue Y116, which directly abuts the F pocket, and its neighboring residue R97. As first observed by Madden et al. (39), the Y116–R97 conformational switch fine-tunes the capacity of the F pocket to the size of the P9 side chain. However, the overall capacity of the A2 binding groove remains constant; thus, this rearrangement can occur only if there is spare capacity in the central region of the binding groove. In the A2-ESO 9C and 1G4 TCR-A2-ESO 9V complexes, peptide residue I6 acts as a secondary anchor, with its side chain bound in the center of the A2 groove. Our crystallographic structure determination revealed that the use of this secondary anchor is maintained in A2-ESO 9L; consequently, the Y116–R97 conformational switch is blocked, precluding any expansion of the F pocket. The longer side chain of leucine cannot be accommodated fully within the F pocket, necessitating an overall upward displacement of the P9 residue relative to its position in other A2-ESO complexes; the change propagates through the peptide to give a distinct shift in main chain position for the entire region between P4 and P9 and, hence, to an altered surface presented for TCR recognition.

ESO 9V is more efficient in inducing conjugate formation and lytic granule polarization than ESO 9L

Formation of conjugates between 1G4 CTL and A2 C1R target cells pulsed with the ESO 9V or the ESO 9L peptide was captured by videomicroscopy. Conjugate formation was faster and more frequent for ESO 9V-pulsed target cells (Supplemental Movie 1) than for ESO 9L-pulsed target cells (Supplemental Movie 2).

To assess the rate of polarization of cytotoxic granules after stimulation of NY-ESO-$1_{157–165}$–specific 1G4 T cells with the ESO 9V or ESO 9L peptide, 1G4 T cells were incubated for 30 min at 37°C with T2 target cells pulsed with different concentrations of the two peptides and then fixed. Anticathepsin D Abs were used to visualize the lytic granules, which were then quantified according to whether the granules and Golgi were localized at the synapse, distal to the synapse, or midway. T2 cells pulsed with ESO 9V peptide were much more efficient in inducing polarization of granules to the synapse in conjugated 1G4 CTLs than T2 cells pulsed with the weaker ESO 9L agonist (Fig. 4*A*, 4*B*). For example, although 10 nM ESO 9V resulted in ~25% of granules being located at the synapse (Fig. 4*A*), 100 nM of the ESO 9L peptide was required to achieve approximately the same effect (Fig. 4*B*). The more efficient lytic granule polarization with the stronger ESO 9V peptide is reflected in the higher percentage of target cell killing seen with ESO 9V compared with ESO 9L (Supplemental Fig. 2).

Examination of the tyrosine phosphorylation patterns induced in the 1G4 CTL clone by stimulation with HLA-A2 tetramers or cell surface presentation of the ESO 9L, ESO 9V, and ESO 9C peptides showed that the main difference in the early membrane proximal signaling induced by the three peptide agonists was associated with the TCR ζ chain. As shown in Supplemental Fig. 3, ESO 9V is very efficient in inducing phosphorylation of TCR ζ when loaded onto HLA-A2 tetramers and when presented at the target cell surface, and it was the only peptide agonist to induce appreciable amounts of phosphorylated linker for activation of T cells (p36). ESO 9L induced ζ phosphorylation only poorly. Supplemental Fig. 4 confirms that HLA-A2 tetramers used in Supplemental Fig. 3*B* were equally folded, as defined by their ability to be recognized by the HLA-A2 conformational specific Ab BB7.2

ESO 9L elicits a lower cytokine response than ESO 9V in 1G4 T cells, which is significantly enhanced by CD8 binding

To examine whether a 6-fold difference in the affinity of 1G4 TCR binding to NY-ESO-$1_{157–165}$ analogs could affect activation of the 1G4 T cell clone, we measured secretion of IFN-γ and MIP-1β by the 1G4 CTL clone stimulated with different concentrations of the

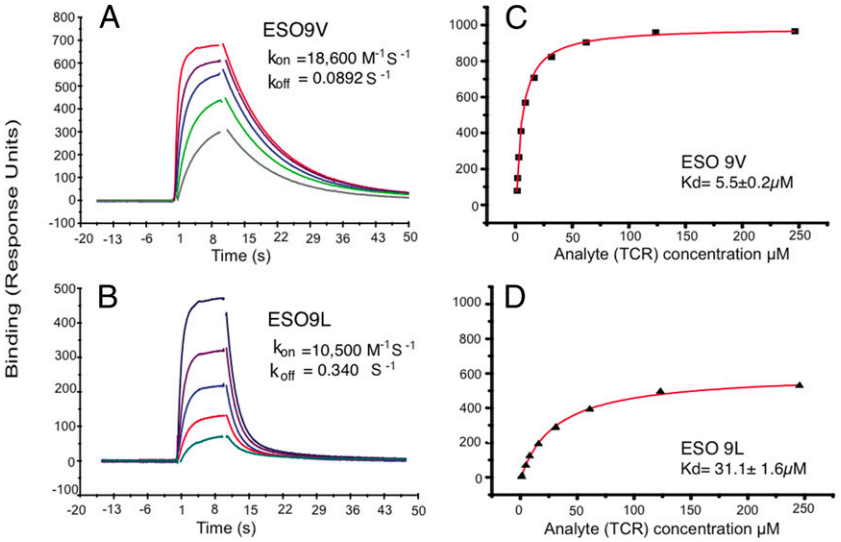

FIGURE 2. Binding of TCR to the pMHC. For kinetic measurements (*A*, *B*), TCR was injected at five concentrations (75 μM, 37.5 μM, 18.8 μM, 9.4 μM, and 4.7 μM as indicated by the different colored traces) over the indicated immobilized peptide-A2 complex. The binding responses for all TCR concentrations are overlaid. The indicated rate constants were determined by global fitting of the 1:1 Langmuir binding model to these data. For affinity measurements (*C*, *D*), TCR was injected over immobilized peptide-A2 complex, and the response was allowed to reach equilibrium. The binding response at equilibrium is plotted against concentration. The 1:1 Langmuir binding model was fitted to the data (solid line) to determine the indicated K_D (mean ± SD of fit).

ESO 9L and ESO 9V peptides, which were loaded onto wild-type A2 C1R target cells (Fig. 5, *left panels*). Consistent with the differences in 1G4 TCR affinities measured by SPR, the level of cytokines secreted by the 1G4 CTL clone sensitized with the ESO 9V peptide was ~50-fold higher than the levels secreted after stimulation with the ESO 9L peptide.

To assess the requirement of CD8 binding in the activation of the 1G4 CTL clone by the ESO 9V and ESO 9L peptides, we compared 1G4 activation by C1R cells expressing the wild-type or CD8-null A2 molecules (i.e., A2 227/228 KA C1R cells) (Fig. 5, *right panels*). Recognition of the ESO 9V peptide is much less dependent on CD8 than recognition of the ESO 9L peptide, because 1G4 T cell activation by the ESO 9L peptide was much more efficient in the presence of A2 molecules bearing a CD8 binding site than the activation of the 1G4 T cells by the ESO 9V peptide. FACS staining of A2 C1R and A2 227/228 KA C1R cells pulsed with different concentrations of the ESO 9V and ESO 9L peptides with the 3M4E5 Ab confirmed that the ESO 9V and ESO 9L peptides bind to A2 and A2 227/228 KA molecules equally well (data not shown).

These results confirm the SPR measurements and indicate that, in the presence of equal A2 loading by the ESO 9L and ESO 9V peptides, the 6-fold difference in binding affinity of the 1G4 TCR to the A2/ESO 9V and A2/ESO 9L complexes results in an ~100-fold difference in the activation of the 1G4 T cell clone.

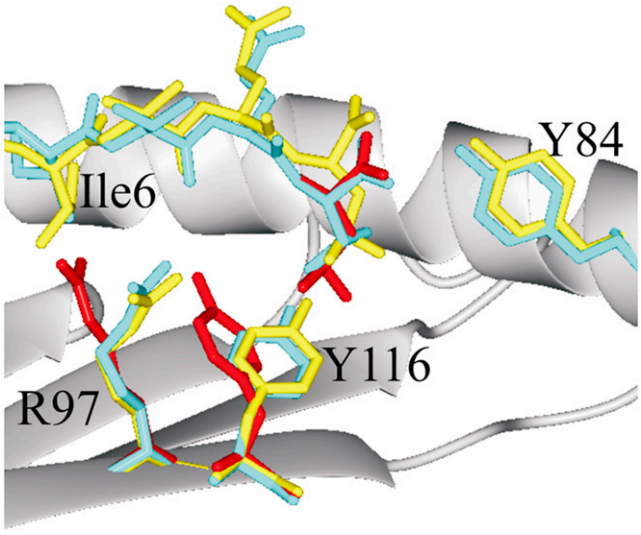

FIGURE 3. Crystal structure of A2-ESO 9L reveals changes in peptide position on substitution of the P9 anchor. The binding groove of A2 is shown schematically as a main chain ribbon (gray), with selected side chains in stick forma. The α2 helix is omitted for clarity, and only the structures containing the peptide residues I-T-Q-C (P6–P9) are shown. The ESO 9L peptide is shown in yellow, and the ESO 9V peptide from the 1G4 TCR-A2-ESO9V complex (PDB code 2BNQ) is shown in cyan. The P9 anchor residue and selected A2 side chains from the A2-SLFNTVATL complex (PDB code 2V2X, a representative P9 leucine anchor peptide-A2 structure) are shown in red and are shown positioned on the A2-ESO 9L structure, in accordance with structural superpositions of the A2 binding grooves.

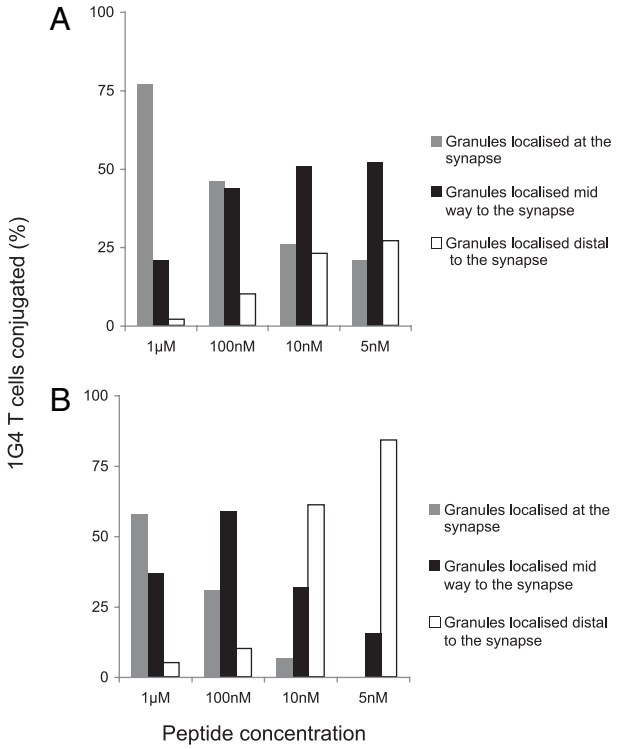

FIGURE 4. Quantitative analysis of granule polarization in the 1G4 CTL clone recognizing targets pulsed with ESO 9V (*A*) or ESO 9L peptides (*B*). Cell conjugates with granules and Golgi localized at the synapse, distal to the synapse, or midway to the synapse were quantified using a fluorescent microscope.

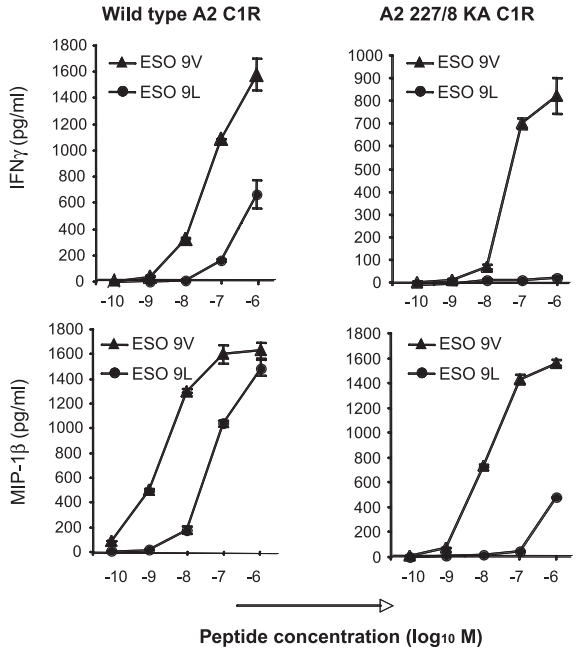

FIGURE 5. Role of CD8 in the recognition of the ESO 9V and ESO 9L peptides. C1R B cells transfected with A2 (wild-type, having a normal interaction with CD8) or A2 227/8 KA (mutant, showing no interaction with CD8) cells were pulsed with the ESO 9V or ESO 9L peptide for 90 min at 37°C. A total of 5×10^4 CTLs were incubated with 5×10^4 pulsed target cells in a total volume of 200 μl in a 96-well plate. Supernatants were harvested and used for ELISA for MIP-1β or IFN-γ.

Different Ca^{2+} influx signatures induced by the ESO 9V and ESO 9L peptides

Having defined the threshold of 1G4 T cell activation, we assessed Ca^{2+} responses at the single-cell level by confocal microscopy upon stimulation by C1R-A2 cells pulsed with different concentrations of the ESO 9V or ESO 9L peptides. C1R-A2 cells pulsed with the influenza matrix$_{58–66}$ peptide served as a negative control. Using 5 or 100 nM ESO 9V peptide resulted in a robust and sustained Ca^{2+} increase (Fig. 6*A*, *upper trace* and data not shown), whereas recognition of the ESO 9L peptide resulted in a less sustained and more oscillatory response (Fig. 6*A*, *lower trace*). The height of the maximum peak of the Ca^{2+} response (F/F_0) was not significantly different between the two peptides, irrespective of the peptide concentration ($p > 0.05$, Fig. 6*B*). However, the change in the mean fluorescence (Δ mean elevated ratio [MER]; an indicator of how sustained the Ca^{2+} influx remains throughout the postengagement period) was consistently higher with ESO 9V than with ESO 9L at peptide concentrations of 5 and 100 nM (Fig. 6*C*). These findings can be accounted for by the nonsustained, oscillatory nature of the ESO 9L-dependent response, which results in a lower mean Ca^{2+} concentration. In terms of population distribution, a large proportion of the 1G4 CTLs responded weakly to 5 nM of the ESO 9L peptide, whereas a larger proportion of the 1G4 CTLs responded more strongly to the same concentration of the ESO 9V peptide (Fig. 6*D*). These differences are preserved with 100-nM peptide, although they are less marked (Fig. 6*E*). No significant Ca^{2+} response was observed with influenza matrix$_{58–66}$ peptide-loaded target cells (data not shown).

To address the contribution of CD8 binding to the overall Ca^{2+} signatures, we then tested the CD8-null C1R A2 227/8KA cells pulsed with ESO 9V or ESO 9L peptide. Recognition of ESO 9V elicited large and sustained Ca^{2+} responses, similar to the responses observed with C1R-A2 cells (Fig. 6*F*, *upper trace*). However, in contrast with the Ca^{2+} responses seen with C1R cells expressing wild-type A2 molecules, C1R A2 227/8KA cells pulsed with ESO 9L peptide evoked only small, oscillatory signals (Fig. 6*F*, *lower trace*), even at the higher peptide concentration (Fig. 6*G*, 6*H*). Indeed, the majority of 1G4 CTLs responded weakly to the ESO 9L peptide, in contrast with the stronger response triggered by the ESO 9V peptide stimulation (Fig. 6*I*, 6*J* and Supplemental Movies 3–6). These functional data demonstrate the importance of the coreceptor CD8 in amplifying the Ca^{2+} signal driven by the weaker ESO 9L peptide, enabling compensation for the lower TCR-pMHC affinity (Fig. 6*B*, 6*C*). In conclusion, these results highlight the ability of individual 1G4 T cells to integrate the affinity of TCR binding and tailor the use of the CD8 coreceptor to the avidity of TCR binding.

We further confirmed the differences in [Ca^{2+}] response to stimulation by the ESO 9V and ESO 9L peptides and by the unmodified ESO 9C peptide by using the ratiometric dye fura 2 at 37°C on a widefield inverted microscope. As shown in Supplemental Fig. 5, the robust and sustained Ca^{2+} release invoked by ESO 9V was apparent in A2 C1R and the CD8-null A2 227/228 KA C1R cells, whereas the response to the ESO 9L peptide was confirmed to be dependent on CD8 expression. Furthermore, the use of this protocol allowed us to rule out the possibility that Ca^{2+} oscillations seen in individual cells when stimulated with the weaker ESO 9L agonist were due to cell movement and were not methodological artifacts, but rather were variations in the Ca^{2+} concentration (Supplemental Fig. 6).

Differences in Ca^{2+} release from the ER evoked by the ESO 9V and ESO 9L peptides

There are two sources of Ca^{2+} that can be used by T cells: intracellular Ca^{2+} stores (Ca^{2+} release) and the extracellular reservoir (Ca^{2+} influx) (16). To dissect their relative contributions to the Ag-induced T cell responses, we performed experiments in Ca^{2+}-free medium (Fig. 7*A–D*), which abolishes Ca^{2+} influx and isolates the intracellular Ca^{2+} release phase (16). In control (Ca^{2+}-containing) medium, Ca^{2+} increased in two phases: an immediate smaller spike, which was followed by a slower, sustained increase (or Ca^{2+} oscillations) (Fig. 7*A–D*). As expected, removing extracellular Ca^{2+} with EGTA confirmed that the first transient peak represents Ca^{2+} release from intracellular stores (Fig. 7*A–D*); clearly, the subsequent response was predominantly Ca^{2+} influx, because Ca^{2+}-free medium abolished this phase in all cases (Fig. 7*A–D*). Therefore, the major difference between stimuli lies in their ability to promote this Ca^{2+} influx (Fig. 7*F*).

The predominant route of Ca^{2+} influx into T cells is the SOCE pathway, which is regulated by the filling state of the intracellular Ca^{2+} stores via a process involving the recently discovered stromal interaction molecule 1 (STIM1) and Orai1 (40, 41). Our data might be explained by the differential emptying of the internal stores, which, in turn, drives a proportional Ca^{2+} influx. Several lines of evidence support such a hypothesis. First, Ca^{2+} release (Fig. 7*E*) and Ca^{2+} influx (Fig. 7*F*) seem to mirror each other, e.g., they are greater for the stronger ESO 9V compared with the weaker ESO 9L stimulus; this difference is more pronounced in the absence of CD8. Moreover, these pooled mean data are a reflection of the underlying single-cell Ca^{2+} signals, which show a significant correlation ($p < 0.001$) between the magnitude of the Ca^{2+} release from stores and the subsequent Ca^{2+} influx for all conditions (Fig. 7*G*). This proportionality of Ca^{2+} store release and Ca^{2+} influx is a hallmark of the SOCE model. Taken together, it emerges that each stimulus evokes a Ca^{2+} release from the ER proportional to the stimulus intensity, which, in turn, drives a proportional Ca^{2+} influx.

To further strengthen the interpretation of our results indicating differential Ca^{2+} release from stores upon T cell stimulation with the

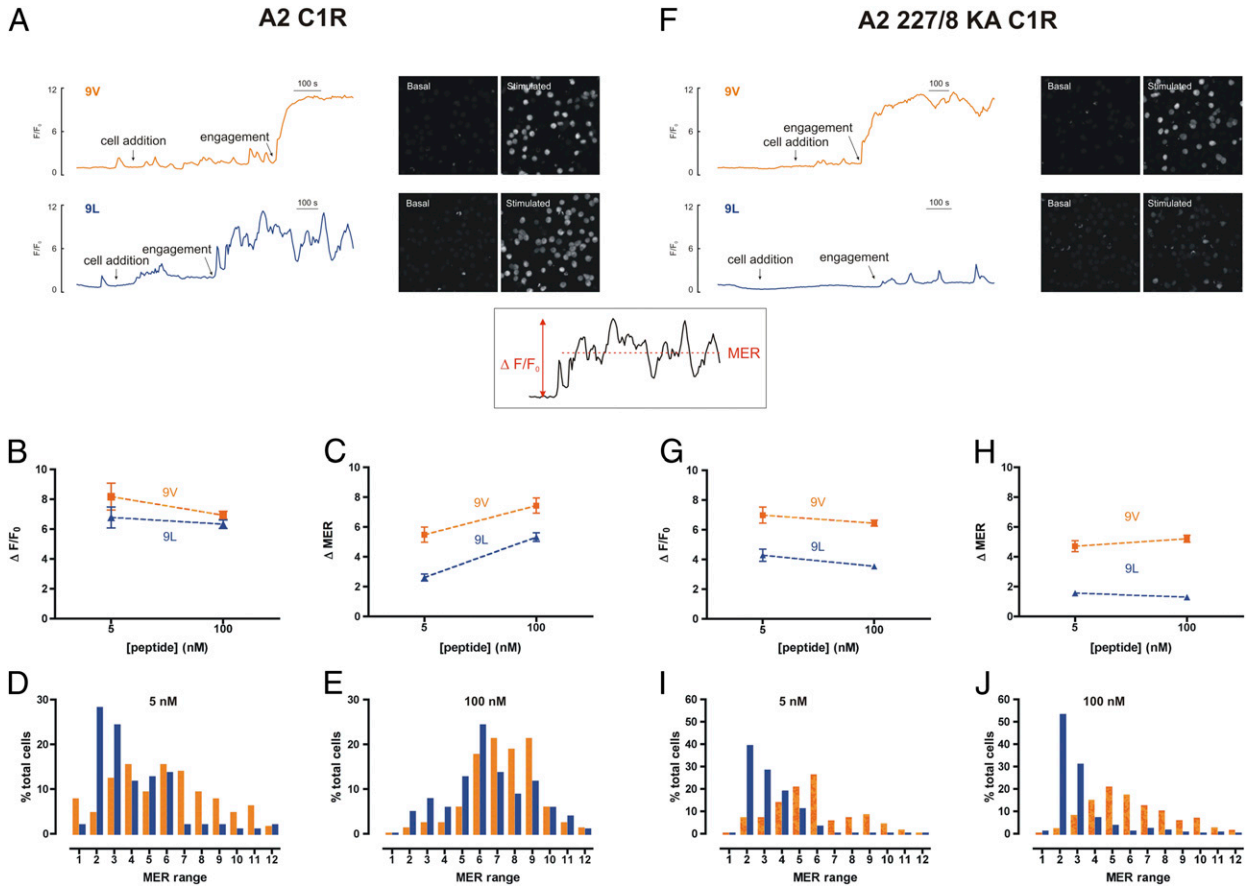

FIGURE 6. Ca^{2+} signals in 1G4 CTLs upon engagement with C1R cells loaded with ESO 9V and ESO 9L peptides. $[Ca^{2+}]_i$ changes were monitored in fluo-3–loaded 1G4 CTLs using a confocal microscope. A2 (*A–E*) or CD8-null 227/8 KA A2 (*F–J*) C1R cells were loaded with ESO 9V or ESO 9L peptide (5 or 100 nM) and added to the chamber ("cell addition"). *A* and *F*, Uncalibrated $[Ca^{2+}]_i$ traces are from representative single cells normalized to initial fluorescence (F/F_0) using 100 nM of the indicated peptide and have been aligned to the time of engagement (TCR–pMHC interaction). Time on the *x*-axis is represented by the scale shown. Basal (initial) and stimulated (final) images of fluo-3 fluorescence of a field of cells depict basal and stimulated $[Ca^{2+}]_i$ and are aligned with the appropriate trace. *B* and *G*, Maximal peak fluorescence changes were determined as the difference between the basal and the maximum fluorescence, $\Delta F/F_0$ (calculated as shown in the inset). *C* and *H*, MER is the mean value of fluorescence throughout the postengagement period, as normalized to F_0. *D*, *E*, *I*, and *J*, Percentage of total 1G4 T cells stimulated with the ESO 9V or ESO 9L peptide with the shown MER value. The MER range is incremented, with the maximum value for each range indicated on the *x*-axis. Data are plotted as the mean ± SEM of 59–104 cells (A2 C1R cells) or 54–260 cells (A2 227/8 AK C1R cells).

different peptides, we used a complementary approach to probe the filling state of the ER by emptying the ER pharmacologically using cyclopiazonic acid (CPA), which inhibits the ER Ca^{2+} pump, resulting in Ca^{2+} leakage from the ER (42). Diagnostic for SOCE, CPA alone empties the ER and activates Ca^{2+} entry (43). To confirm that the ER was fully emptied by CPA, the Ca^{2+} ionophore, ionomycin, was subsequently applied, demonstrating little further effect, as shown in (Fig. 8*G*). We then went on to test the ER Ca^{2+} store size using CPA after stimulating the 1G4 T cell clone with the ESO 9V or ESO 9L peptide, in the presence or absence of CD8 binding (the mean Ca^{2+} responses were quantified as depicted in Fig. 8*H*). We observed that 1G4 T cells stimulated by the stronger ESO 9V peptide agonist emptied the intracellular stores almost completely, because CPA and ionomycin had little further effect on Ca^{2+} release (Fig. 8*C*, 8*E*). In contrast, the weaker ESO 9L peptide agonist failed to empty the stores completely, as shown by the greater increase in Ca^{2+} release after the addition of CPA and ionomycin (Fig. 8*A*, 8*E*). Consistent with the results shown in Fig. 6, the absence of CD8 binding to the A2 227/8KA cells compromised the Ca^{2+} release from stores after stimulation with the weaker ESO 9L, and a large residual Ca^{2+} content was revealed by CPA (Fig. 8*B*, 8*F*). In contrast, Ca^{2+} store depletion was still large with the ESO 9V peptide, even in the absence of CD8 coreceptors, as evidenced by the small response to CPA and ionomycin (Fig. 8*D*, 8*F*). The reciprocal relationship between the responses to Ag and to CPA is consistent with a common pathway and further reinforces our SOCE hypothesis.

Taken together, these results further support the conclusion that the strength of TCR affinity stimulates differential egress of Ca^{2+} release from intracellular stores, which, in turn, drives a proportional Ca^{2+} influx.

Discussion

Our results demonstrate that the amount of Ca^{2+} released from intracellular stores is dependent on the strength of TCR stimulation and can be modulated by CD8 binding to pMHCs. Although strong agonist peptides are capable of depleting the ER of Ca^{2+}, even in the absence of CD8 binding to pMHC, T cell activation by weaker peptide agonists requires CD8 binding to pMHC to enhance the amount of Ca^{2+} released from the ER, resulting in greater Ca^{2+} influx from the extracellular environment and significantly more efficient T cell activation.

By applying a combination of structural, kinetic, and functional analyses, we characterized two peptide analogs of the wild-type NY-ESO-$1_{157–165}$ tumor Ag peptide—the ESO 9V and ESO 9L

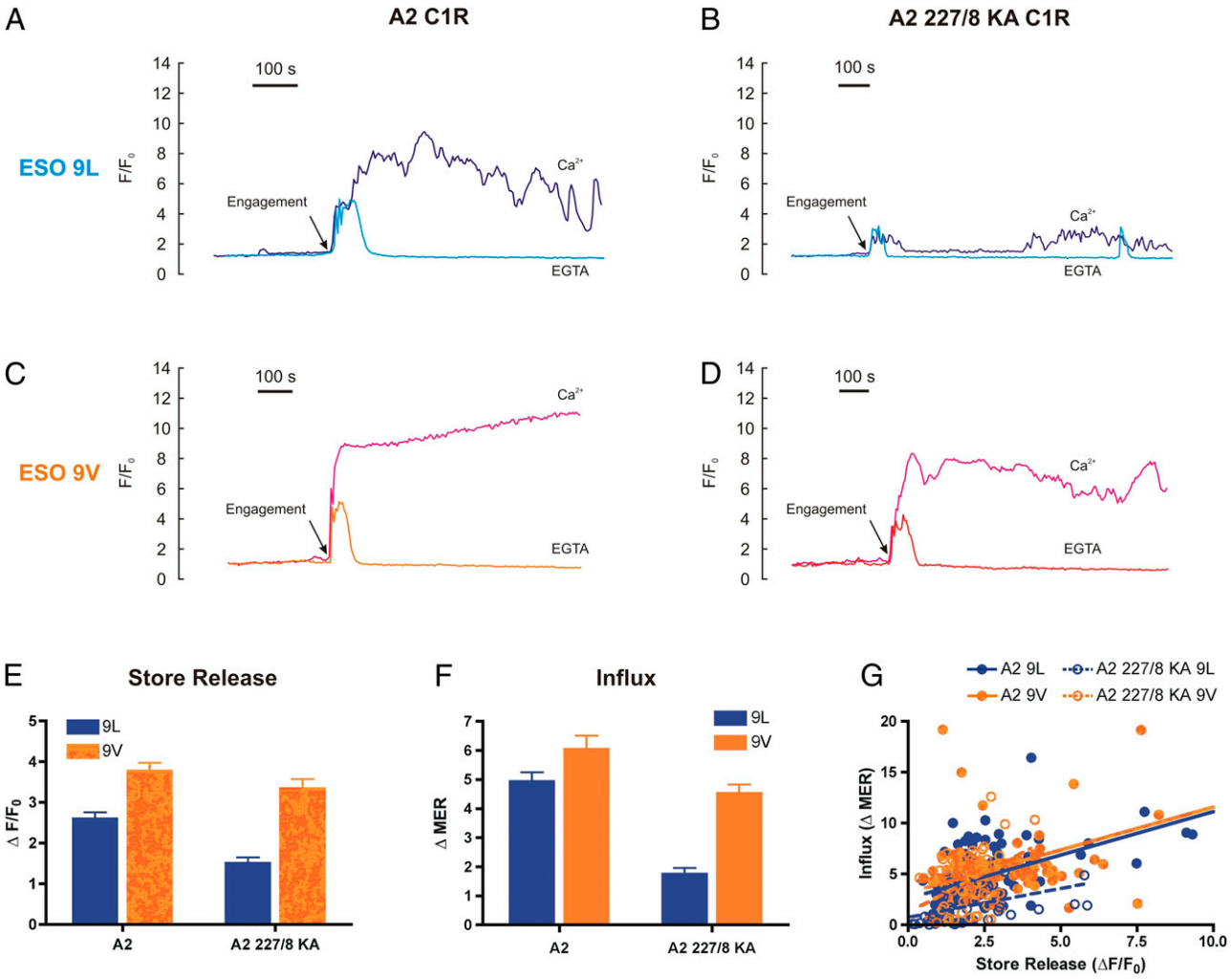

FIGURE 7. The relative contribution of intracellular Ca^{2+} release and Ca^{2+} influx to the 1G4 CTL response. 1G4 CTL $[Ca^{2+}]_i$ responses were monitored with fluo-3, as described previously. Before cell addition (not shown), C1R cells and 1G4 CTLs were washed in Ca^{2+}-free medium supplemented with 1 mM EGTA to remove all traces of extracellular Ca^{2+}, and experiments were conducted in the same medium where indicated (EGTA). In parallel, control cells were maintained throughout in Ca^{2+}-containing medium (0.5 mM, as for RPMI 1640, Ca^{2+}). *A–D*, Traces from representative single cells normalized to initial fluorescence (F/F_0) using 100 nM of the indicated peptide under either condition (Ca^{2+} or EGTA) and manually aligned to the time of engagement (TCR–pMHC interaction). Time on the *x*-axis is represented by the scale shown. *E* and *F*, Summary of the responses in EGTA-containing medium. *E*, Amplitude of the initial Ca^{2+} release from intracellular stores. *F*, Subsequent Ca^{2+} influx quantified as the total postengagement ΔMER. Data are mean intracellular Ca^{2+} signal in the presence of EGTA expressed as a percentage of the parallel control in the presence of extracellular Ca^{2+}. Data in *E* and *F* are expressed as the mean ± SEM of *n* single cells ($n = 102$ [A2, ESO9L]; $n = 113$ [A2, ESO9V]; $n = 68$ [A2 227/8, ESO9L]; and $n = 63$ [A2 227/8, ESO9V]). *G*, Correlation analysis in which data are fitted by linear regression. A significant correlation was observed for all data sets ($p < 0.001$) with r^2 values of +0.40 (A2, ESO9L), +0.41 (A2, ESO9V), +0.22 (A2 227/8, ESO9L), and +0.20 (A2 227/8, ESO9V).

peptides—which have a very similar affinity for A2 molecules and differ by only 6-fold in their affinity to the 1G4 TCR. This model provided us with the opportunity to study the activation of the 1G4 T cell clone by the strong (ESO 9V) or weak (ESO 9L) peptide and interpret its differential activation as a direct effect of the two peptides' affinity of binding to the 1G4 TCR, which is being used by several groups to study the relationship between TCR mutagenesis, affinity to pMHC, and T cell activation (7, 9, 33, 44, 45).

A high-resolution structure (1.65 Å) of unliganded A2 molecules loaded with the ESO 9L peptide demonstrated that the overall structure of the ESO 9L epitope in A2 is similar to the structure of the 1G4 liganded A2-ESO 9V (33) and unliganded A2-ESO 9C complexes (38). The analysis of the A2-ESO 9L crystal structure revealed an overall upward displacement of the P9 residue relative to its position in the ESO 9V peptide due to the blocked Y116–R97 conformational switch, which precludes any expansion of the F pocket. It is likely that such subtle, indirectly triggered changes in the pMHC surface may account for the 6-fold variation in binding affinity between the 1G4 TCR and the ESO 9V and ESO 9L peptides, because similar changes in the pMHC surface were shown to alter TCR binding properties in a number of pMHC-TCR systems (46).

Analysis of cytokine secretion released by the 1G4 T clone stimulated by the ESO 9V or ESO 9L peptide in the presence or absence of CD8 binding allowed us to define the threshold of activation of the 1G4 T cell clone by strong or weak stimuli, as well as to confirm that T cell stimulation by strong stimuli is less dependent on the use of the coreceptor CD8.

After characterizing the threshold of 1G4 activation by strong and weak stimuli, we analyzed the pattern of Ca^{2+} signals evoked by two concentrations (5 and 100 nM) of ESO 9L and ESO 9V peptides in the presence or absence of CD8 binding. The results of these experiments confirmed that the pattern of the Ca^{2+} signals can be modulated by the strength of TCR stimulation and by the binding of

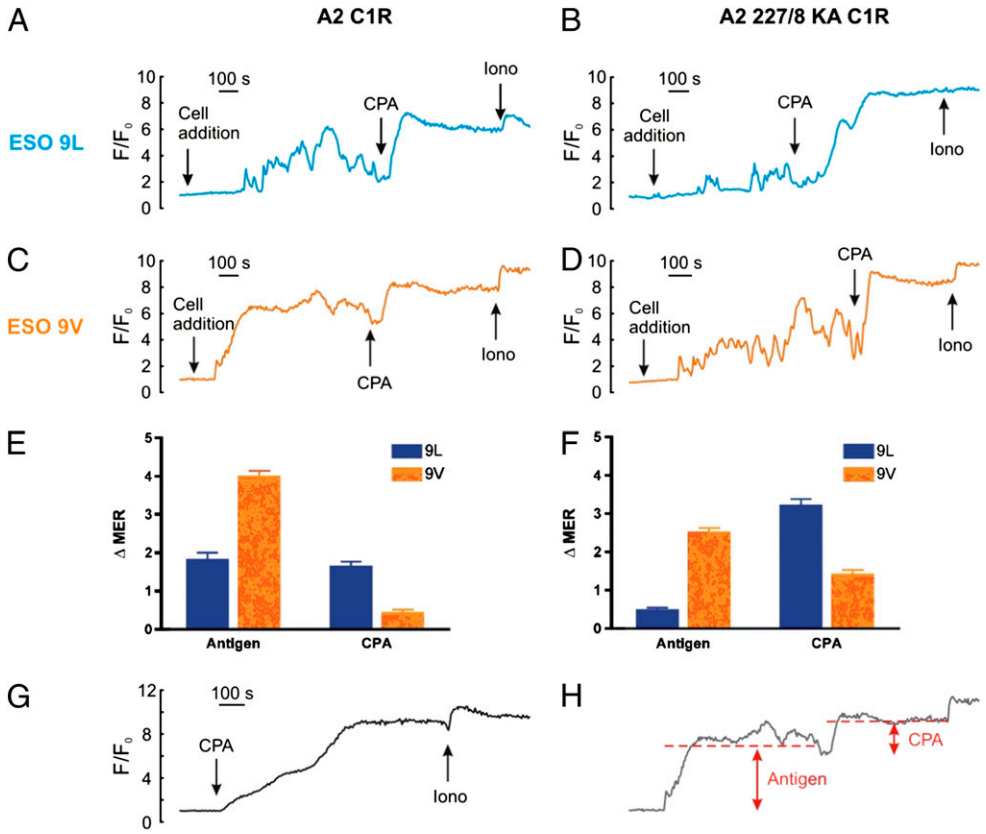

FIGURE 8. Probing the Ca^{2+} store-filling status with the Ca^{2+} pump inhibitor CPA. 1G4 CTLs were stimulated with C1R A2 and C1R A2 227/8 KA cells pulsed with 100 nM ESO 9V or ESO 9L peptide as described previously; subsequently, they were treated with 30 μM CPA and 5 μM ionomycin as indicated (*A–D*). Control cells were treated with CPA and ionomycin only (*G*). *H*, Schematic diagram illustrating how the traces were measured, with the dotted line showing the MER compared with F/F_0 immediately prior to the additions. Data were quantified by measuring the change in the mean Ca^{2+} response, as shown in *E* and *F*, and expressed as the mean ± SEM of *n* single cells ($n = 71$ [A2, ESO9L]; $n = 105$ [A2, ESO9V]; $n = 79$ [A2 227/8, ESO9L]; and $n = 88$ [A2 227/8, ESO9V]). Time on the *x*-axis is represented by the scale shown.

the coreceptor CD8 to MHC class I molecules. Our data unequivocally demonstrate that the Ca^{2+} signals elicited by the ESO 9V peptide are more robust and sustained than those evoked with ESO 9L. The increase in TCR-dependent cytosolic Ca^{2+} in T cells serves a number of functions in the short- and long-term (47–49): Ca^{2+} signals are associated with motility, T cell proliferation, and changes in T cell gene expression and secretion of cytokines; the pattern of these signals determines T cell polarization, fitness, and life span. For example, more sustained Ca^{2+} responses favor activation of NF-AT, JNK, and IL-2 expression, whereas lower Ca^{2+} signals promote NF-κB activation (15, 50, 51).

By investigating what underlies these Ca^{2+} signatures, we propose a model whereby the strength of the pMHC–TCR interaction dictates the degree of ER Ca^{2+} store depletion, which, in turn, drives a proportional activation of SOCE. Such a model is supported by various aspects of our data: the abolition of Ca^{2+} influx (by using Ca^{2+}-free medium) confirmed that the initial Ca^{2+} phase was derived from intracellular stores; this Ca^{2+} release represented only a minor (but crucial) contributor to the Ca^{2+} signature, which was otherwise dominated by Ca^{2+} influx; and this Ca^{2+} influx was proportional to the degree of store emptying (as assessed by two independent means). Overall, the stronger stimuli evoked a substantial depletion of stores and a marked Ca^{2+} influx, whereas both phases were proportionally smaller for the weaker stimuli.

In terms of the underlying cell signaling, it has been suggested that TCR stimulation leads to the production of various Ca^{2+}-mobilizing second messengers: inositol 1,4,5-trisphosphate (IP_3), cyclic ADP-ribose, and nicotinic acid adenine dinucleotide phosphate (NAADP) (52). Each messenger can evoke Ca^{2+} release from internal stores by activating its own unique cognate receptor: IP_3 receptors, ryanodine receptors, and two-pore channels (NAADP receptors), respectively (53). Although the role of IP_3 receptors in TCR-mediated responses was reported (16, 54), it remains unclear whether the other second messengers (cyclic ADP-ribose and NAADP) are involved in the response of T cell clones by cognate peptide agonists, because only Jurkat T cells activated by anti-CD3 Ab treatment have been tested (55–57).

Following this first phase, Ca^{2+} influx ensues as a result of the recruitment of the SOCE pathway, operated via the opening of calcium release-activated channels/Orai1 located at the T cell surface (13, 14), which are linked to ER Ca^{2+} store emptying through the ER-resident Ca^{2+} sensor STIM1 (14, 47, 48). We contend that the Orai/STIM1 complex is differentially activated by the different peptides we used, but this requires experimental confirmation. Although we acknowledge that other factors can influence the Ca^{2+} influx phase, such as plasma membrane Ca^{2+} pumps (58) or changes in membrane potential (47, 59), the fact that CPA responses reach a similar plateau after any Ag tends to discount them as the major influence. Therefore, we conclude that different Ags evoke different Ca^{2+} influx signals as a consequence of different Ca^{2+} release from internal stores.

We also showed that the CD8 coreceptor influences the release of Ca^{2+} from the ER and the overall pattern of Ca^{2+} influx. Although for strong stimuli, the presence or absence of CD8 binding did not significantly alter the release of Ca^{2+} from the stores, the amount of Ca^{2+} released from the stores in response to weaker stimuli was

enhanced by CD8 binding to MHC class I molecules. It is known that CD8 binding to MHC class I molecules is important for stabilizing the interaction between low-affinity TCRs and MHC class I molecules (60, 61) and for controlling the dynamics of CTL activation and immunological synapse formation (62). In addition, it was shown that lymphokines can regulate the level of CD8 coreceptor expression (63). We showed that binding of the CD8 coreceptor to MHC class I molecules influences the release of Ca^{2+} influx. These results provide further evidence that T cells are able to integrate the strength of TCR signals and tailor the use of coreceptors to increase the avidity of the TCR–pMHC interaction for a weaker ligand so that the T cell activation threshold is exceeded. This latter finding is consistent with the results of a recently published report indicating that T cells can "sense" the affinity of cognate peptide by fine-tuning the duration of T cell interaction with target cells, depending on the dose of peptides presented on the surface of target cells (64), and of integrating TCR-dependent signals by tailoring the use of the coreceptor CD8 to reach a set threshold of activation.

In conclusion, our data highlight the correlation between TCR affinity and the release of Ca^{2+} from intracellular stores. This effect is further enhanced by the binding of the coreceptor CD8 to MHC class I molecules, indicating that T cells are capable of "sensing" the affinity of peptide agonists and determining their requirement for a coreceptor, such as CD8, in the context of weak peptide agonists, to ensure T cell activation. Together, these data provide important insights into the mechanisms controlling the activation of melanoma-specific $CD8^+$ T cells, underscoring the ability of T cells to recruit the CD8 coreceptor to enhance Ca^{2+} release from the ER in the context of weak peptide agonists, thus ensuring an appropriate T cell response. This ability to modulate the strength of T cell interaction by the recruitment of coreceptors ensures that individual T cells can recognize a broader pool of self and nonself peptides. This has implications for the use of altered peptide ligands and mutagenized TCRs in adoptively transferred tumor-specific $CD4^+$ and $CD8^+$ T cells, and it may be important for modulation of the immune response to self-Ags in autoimmune disorders and for cross-reactivity between virus serotypes, such as in the recognition of rapidly mutating HIV-1 escape variants.

Acknowledgments

We thank the staff of the European Synchrotron Radiation Facility and the European Molecular Biology Laboratory outstation at Grenoble for assistance with data collection. Crystallization trials were carried out using facilities provided by the Oxford Protein Production Facility and the European Commission Integrated Programme Structural Proteomics in Europe (QLG2-CT-2002-00988). We thank Oreste Acuto for critically reading the manuscript and Moira Johnson for editing the manuscript.

Disclosures

The authors have no financial conflicts of interest.

References

1. Rosenberg, S. A., J. C. Yang, D. J. Schwartzentruber, P. Hwu, F. M. Marincola, S. L. Topalian, N. P. Restifo, M. E. Dudley, S. L. Schwarz, P. J. Spiess, et al. 1998. Immunologic and therapeutic evaluation of a synthetic peptide vaccine for the treatment of patients with metastatic melanoma. *Nat. Med.* 4: 321–327.
2. Chen, J. L., P. R. Dunbar, U. Gileadi, E. Jäger, S. Gnjatic, Y. Nagata, E. Stockert, D. L. Panicali, Y. T. Chen, A. Knuth, et al. 2000. Identification of NY-ESO-1 peptide analogues capable of improved stimulation of tumor-reactive CTL. *J. Immunol.* 165: 948–955.
3. Romero, P., V. Dutoit, V. Rubio-Godoy, D. Liénard, D. Speiser, P. Guillaume, K. Servis, D. Rimoldi, J. C. Cerottini, and D. Valmori. 2001. CD8+ T-cell response to NY-ESO-1: relative antigenicity and in vitro immunogenicity of natural and analogue sequences. *Clin. Cancer Res.* 7: (3):, Suppl.)766s–772s.
4. Schumacher, T. N., and N. P. Restifo. 2009. Adoptive T cell therapy of cancer. *Curr. Opin. Immunol.* 21: 187–189.
5. Valmori, D., J. F. Fonteneau, C. M. Lizana, N. Gervois, D. Liénard, D. Rimoldi, V. Jongeneel, F. Jotereau, J. C. Cerottini, and P. Romero. 1998. Enhanced generation of specific tumor-reactive CTL in vitro by selected Melan-A/MART-1 immunodominant peptide analogues. *J. Immunol.* 160: 1750–1758.
6. Parkhurst, M. R., M. L. Salgaller, S. Southwood, P. F. Robbins, A. Sette, S. A. Rosenberg, and Y. Kawakami. 1996. Improved induction of melanoma-reactive CTL with peptides from the melanoma antigen gp100 modified at HLA-A*0201-binding residues. *J. Immunol.* 157: 2539–2548.
7. Robbins, P. F., Y. F. Li, M. El-Gamil, Y. Zhao, J. A. Wargo, Z. Zheng, H. Xu, R. A. Morgan, S. A. Feldman, L. A. Johnson, et al. 2008. Single and dual amino acid substitutions in TCR CDRs can enhance antigen-specific T cell functions. *J. Immunol.* 180: 6116–6131.
8. Iero, M., P. Filipazzi, C. Castelli, F. Belli, R. Valdagni, G. Parmiani, R. Patuzzo, M. Santinami, and L. Rivoltini. 2009. Modified peptides in anti-cancer vaccines: are we eventually improving anti-tumour immunity? *Cancer Immunol. Immunother.* 58: 1159–1167.
9. Purbhoo, M. A., D. H. Sutton, J. E. Brewer, R. E. Mullings, M. E. Hill, T. M. Mahon, J. Karbach, E. Jäger, B. J. Cameron, N. Lissin, et al. 2006. Quantifying and imaging NY-ESO-1/LAGE-1-derived epitopes on tumor cells using high affinity T cell receptors. *J. Immunol.* 176: 7308–7316.
10. Gallo, E. M., K. Canté-Barrett, and G. R. Crabtree. 2006. Lymphocyte calcium signaling from membrane to nucleus. *Nat. Immunol.* 7: 25–32.
11. Huse, M., L. O. Klein, A. T. Girvin, J. M. Faraj, Q. J. Li, M. S. Kuhns, and M. M. Davis. 2007. Spatial and temporal dynamics of T cell receptor signaling with a photoactivatable agonist. *Immunity* 27: 76–88.
12. Huang, Y., and R. L. Wange. 2004. T cell receptor signaling: beyond complex complexes. *J. Biol. Chem.* 279: 28827–28830.
13. Parekh, A. B., and J. W. Putney, Jr. 2005. Store-operated calcium channels. *Physiol. Rev.* 85: 757–810.
14. Lewis, R. S. 2007. The molecular choreography of a store-operated calcium channel. *Nature* 446: 284–287.
15. Dolmetsch, R. E., K. Xu, and R. S. Lewis. 1998. Calcium oscillations increase the efficiency and specificity of gene expression. *Nature* 392: 933–936.
16. Lewis, R. S. 2001. Calcium signaling mechanisms in T lymphocytes. *Annu. Rev. Immunol.* 19: 497–521.
17. Chen, Y. Z., Z. F. Lai, K. Nishi, and Y. Nishimura. 1998. Modulation of calcium responses by altered peptide ligands in a human T cell clone. *Eur. J. Immunol.* 28: 3929–3939.
18. Sloan-Lancaster, J., T. H. Steinberg, and P. M. Allen. 1996. Selective activation of the calcium signaling pathway by altered peptide ligands. *J. Exp. Med.* 184: 1525–1530.
19. Wülfing, C., J. D. Rabinowitz, C. Beeson, M. D. Sjaastad, H. M. McConnell, and M. M. Davis. 1997. Kinetics and extent of T cell activation as measured with the calcium signal. *J. Exp. Med.* 185: 1815–1825.
20. König, R., L.Y. Huang, and R.N. Germain. 1992. MHC class II interaction with CD4 mediated by a region analogous to the MHC class I binding site for CD8. *Nature* 356: 796–798.
21. Salter, R. D., R. J. Benjamin, P. K. Wesley, S. E. Buxton, T. P. Garrett, C. Clayberger, A. M. Krensky, A. M. Norment, D. R. Littman, and P. Parham. 1990. A binding site for the T-cell co-receptor CD8 on the α3 domain of HLA-A2. *Nature* 345: 41–46.
22. Norment, A. M., R. D. Salter, P. Parham, V. H. Engelhard, and D. R. Littman. 1988. Cell-cell adhesion mediated by CD8 and MHC class I molecules. *Nature* 336: 79–81.
23. Cole, D. K., S. M. Dunn, M. Sami, J. M. Boulter, B. K. Jakobsen, and A. K. Sewell. 2008. T cell receptor engagement of peptide-major histocompatibility complex class I does not modify CD8 binding. *Mol. Immunol.* 45: 2700–2709.
24. Gallagher, P. F., B. Fazekas de St Groth, and J. F. Miller. 1989. CD4 and CD8 molecules can physically associate with the same T-cell receptor. *Proc. Natl. Acad. Sci. USA* 86: 10044–10048.
25. Leitenberg, D., Y. Boutin, S. Constant, and K. Bottomly. 1998. CD4 regulation of TCR signaling and T cell differentiation following stimulation with peptides of different affinities for the TCR. *J. Immunol.* 161: 1194–1203.
26. Veillette, A., M. A. Bookman, E. M. Horak, and J. B. Bolen. 1988. The CD4 and CD8 T cell surface antigens are associated with the internal membrane tyrosine-protein kinase p56lck. *Cell* 55: 301–308.
27. Zamoyska, R. 1998. CD4 and CD8: modulators of T-cell receptor recognition of antigen and of immune responses? *Curr. Opin. Immunol.* 10: 82–87.
28. Ehrlich, L. I., P. J. Ebert, M. F. Krummel, A. Weiss, and M. M. Davis. 2002. Dynamics of p56lck translocation to the T cell immunological synapse following agonist and antagonist stimulation. *Immunity* 17: 809–822.
29. Lewis, L. A., C. D. Chung, J. Chen, J. R. Parnes, M. Moran, V. P. Patel, and M. C. Miceli. 1997. The Lck SH2 phosphotyrosine binding site is critical for efficient TCR-induced processive tyrosine phosphorylation of the ζ-chain and IL-2 production. *J. Immunol.* 159: 2292–2300.
30. van Oers, N. S. C., N. Killeen, and A. Weiss. 1996. Lck regulates the tyrosine phosphorylation of the T cell receptor subunits and ZAP-70 in murine thymocytes. *J. Exp. Med.* 183: 1053–1062.
31. Iwashima, M., B. A. Irving, N. S. van Oers, A. C. Chan, and A. Weiss. 1994. Sequential interactions of the TCR with two distinct cytoplasmic tyrosine kinases. *Science* 263: 1136–1139.
32. LoGrasso, P. V., J. Hawkins, L. J. Frank, D. Wisniewski, and A. Marcy. 1996. Mechanism of activation for Zap-70 catalytic activity. *Proc. Natl. Acad. Sci. USA* 93: 12165–12170.
33. Chen, J. L., G. Stewart-Jones, G. Bossi, N. M. Lissin, L. Wooldridge, E. M. Choi, G. Held, P. R. Dunbar, R. M. Esnouf, M. Sami, et al. 2005. Structural

and kinetic basis for heightened immunogenicity of T cell vaccines. *J. Exp. Med.* 201: 1243–1255.
34. Otwinowski, Z., and W. Minor. 1997. Processing of X-ray diffraction data collected in oscillation mode. *Methods Enzymol.* 276: 307–326.
35. Murshudov, G. N., A. A. Vagin, and E. J. Dodson. 1997. Refinement of macromolecular structures by the maximum-likelihood method. *Acta Crystallogr. D Biol. Crystallogr.* 53: 240–255.
36. Emsley, P., and K. Cowtan. 2004. Coot: model-building tools for molecular graphics. *Acta Crystallogr. D Biol. Crystallogr.* 60: 2126–2132.
37. Morris, R. J., A. Perrakis, and V. S. Lamzin. 2002. ARP/wARP's model-building algorithms. I. The main chain. *Acta Crystallogr. D Biol. Crystallogr.* 58: 968–975.
38. Webb, A. I., M. A. Dunstone, W. Chen, M. I. Aguilar, Q. Chen, H. Jackson, L. Chang, L. Kjer-Nielsen, T. Beddoe, J. McCluskey, et al. 2004. Functional and structural characteristics of NY-ESO-1-related HLA A2-restricted epitopes and the design of a novel immunogenic analogue. *J. Biol. Chem.* 279: 23438–23446.
39. Madden, D. R., D. N. Garboczi, and D. C. Wiley. 1993. The antigenic identity of peptide-MHC complexes: a comparison of the conformations of five viral peptides presented by HLA-A2. *Cell* 75: 693–708.
40. Luik, R. M., and R. S. Lewis. 2007. New insights into the molecular mechanisms of store-operated Ca2+ signaling in T cells. *Trends Mol. Med.* 13: 103–107.
41. Feske, S. 2007. Calcium signalling in lymphocyte activation and disease. *Nat. Rev. Immunol.* 7: 690–702.
42. Morgan, A. J., and R. Jacob. 1998. Differential modulation of the phases of a Ca2+ spike by the store Ca2+-ATPase in human umbilical vein endothelial cells. *J. Physiol.* 513: 83–101.
43. Luik, R. M., B. Wang, M. Prakriya, M. M. Wu, and R. S. Lewis. 2008. Oligomerization of STIM1 couples ER calcium depletion to CRAC channel activation. *Nature* 454: 538–542.
44. Li, Y., R. Moysey, P. E. Molloy, A. L. Vuidepot, T. Mahon, E. Baston, S. Dunn, N. Liddy, J. Jacob, B. K. Jakobsen, and J. M. Boulter. 2005. Directed evolution of human T-cell receptors with picomolar affinities by phage display. *Nat. Biotechnol.* 23: 349–354.
45. Zhao, Y., A. D. Bennett, Z. Zheng, Q. J. Wang, P. F. Robbins, L. Y. Yu, Y. Li, P. E. Molloy, S. M. Dunn, B. K. Jakobsen, et al. 2007. High-affinity TCRs generated by phage display provide CD4+ T cells with the ability to recognize and kill tumor cell lines. *J. Immunol.* 179: 5845–5854.
46. Luz, J. G., M. Huang, K. C. Garcia, M. G. Rudolph, V. Apostolopoulos, L. Teyton, and I. A. Wilson. 2002. Structural comparison of allogeneic and syngeneic T cell receptor-peptide-major histocompatibility complex complexes: a buried alloreactive mutation subtly alters peptide presentation substantially increasing V_β interactions. *J. Exp. Med.* 195: 1175–1186.
47. Vig, M., and J. P. Kinet. 2009. Calcium signaling in immune cells. *Nat. Immunol.* 10: 21–27.
48. Oh-hora, M., and A. Rao. 2008. Calcium signaling in lymphocytes. *Curr. Opin. Immunol.* 20: 250–258.
49. Stinchcombe, J. C., E. Majorovits, G. Bossi, S. Fuller, and G. M. Griffiths. 2006. Centrosome polarization delivers secretory granules to the immunological synapse. *Nature* 443: 462–465.
50. Dolmetsch, R. E., R. S. Lewis, C. C. Goodnow, and J. I. Healy. 1997. Differential activation of transcription factors induced by Ca2+ response amplitude and duration. *Nature* 386: 855–858.
51. Zhong, F., M. C. Davis, K. S. McColl, and C. W. Distelhorst. 2006. Bcl-2 differentially regulates Ca2+ signals according to the strength of T cell receptor activation. *J. Cell Biol.* 172: 127–137.
52. Morgan, A. J., G. C. Churchill, R. Masgrau, M. Ruas, L. C. Davis, R. A. Billington, S. Patel, M. Yamasaki, J. M. Thomas, A. A. Genazzani, and A. Galione. 2006. Methods in cADPR and NAADP research. In *Methods in Calcium Signalling*. J. W. Putney, Jr., ed. CRC Press, Boca Raton, FL. p. 265–334.
53. Calcraft, P. J., M. Ruas, Z. Pan, X. Cheng, A. Arredouani, X. Hao, J. Tang, K. Rietdorf, L. Teboul, K. T. Chuang, et al. 2009. NAADP mobilizes calcium from acidic organelles through two-pore channels. *Nature* 459: 596–600.
54. Treves, S., F. Di Virgilio, V. Cerundolo, P. Zanovello, D. Collavo, and T. Pozzan. 1987. Calcium and inositolphosphates in the activation of T cell-mediated cytotoxicity. *J. Exp. Med.* 166: 33–42.
55. Schwarzmann, N., S. Kunerth, K. Weber, G. W. Mayr, and A. H. Guse. 2002. Knock-down of the type 3 ryanodine receptor impairs sustained Ca2+ signaling via the T cell receptor/CD3 complex. *J. Biol. Chem.* 277: 50636–50642.
56. Steen, M., T. Kirchberger, and A. H. Guse. 2007. NAADP mobilizes calcium from the endoplasmic reticular Ca(2+) store in T-lymphocytes. *J. Biol. Chem.* 282: 18864–18871.
57. Guse, A. H., C. P. da Silva, I. Berg, A. L. Skapenko, K. Weber, P. Heyer, M. Hohenegger, G. A. Ashamu, H. Schulze-Koops, B. V. Potter, and G. W. Mayr. 1999. Regulation of calcium signalling in T lymphocytes by the second messenger cyclic ADP-ribose. *Nature* 398: 70–73.
58. Madge, L., I. C. Marshall, and C. W. Taylor. 1997. Delayed autoregulation of the Ca2+ signals resulting from capacitative Ca2+ entry in bovine pulmonary artery endothelial cells. *J. Physiol.* 498: 351–369.
59. Donnadieu, E., G. Bismuth, and A. Trautmann. 1992. Calcium fluxes in T lymphocytes. *J. Biol. Chem.* 267: 25864–25872.
60. Choi, E. M., J. L. Chen, L. Wooldridge, M. Salio, A. Lissina, N. Lissin, I. F. Hermans, J. D. Silk, F. Mirza, M. J. Palmowski, et al. 2003. High avidity antigen-specific CTL identified by CD8-independent tetramer staining. *J. Immunol.* 171: 5116–5123.
61. Laugel, B., D. A. Price, A. Milicic, and A. K. Sewell. 2007. CD8 exerts differential effects on the deployment of cytotoxic T lymphocyte effector functions. *Eur. J. Immunol.* 37: 905–913.
62. Purbhoo, M. A., D. J. Irvine, J. B. Huppa, and M. M. Davis. 2004. T cell killing does not require the formation of a stable mature immunological synapse. *Nat. Immunol.* 5: 524–530.
63. Park, J. H., S. Adoro, P. J. Lucas, S. D. Sarafova, A. S. Alag, L. L. Doan, B. Erman, X. Liu, W. Ellmeier, R. Bosselut, et al. 2007. 'Coreceptor tuning': cytokine signals transcriptionally tailor CD8 coreceptor expression to the self-specificity of the TCR. *Nat. Immunol.* 8: 1049–1059.
64. Henrickson, S. E., T. R. Mempel, I. B. Mazo, B. Liu, M. N. Artyomov, H. Zheng, A. Peixoto, M. P. Flynn, B. Senman, T. Junt, et al. 2008. T cell sensing of antigen dose governs interactive behavior with dendritic cells and sets a threshold for T cell activation. *Nat. Immunol.* 9: 282–291.